Factors Governing the Magnetoresistance Properties of the Electron-Doped Manganites $Ca_{1-x}A_xMnO_3$ (A = Ln, Th)

A. Maignan,* C. Martin, F. Damay, and B. Raveau

Laboratoire CRISMAT, UMR 6508 associée au CNRS, ISMRA et Université de Caen, 6, Boulevard du Maréchal Juin, 14050 Caen Cedex, France

Received December 2, 1997
Revised Manuscript Received February 17, 1998

Introduction

A great deal of work has been devoted to the hole-doped manganites with the perovskite structure these last years, owing to their spectacular colossal magnetoresistance (CMR) properties. In contrast, very few investigations were performed on the electron-doped manganites, corresponding to Mn(IV)-rich perovskites. The results obtained for the perovskites $Bi_{1-x}Ca_xMnO_3$, with x ranging from 0.75 to 0.90,[1−4] show that the magnetic and transport properties of these Mn(IV)-rich manganites are of great interest. For $0.74 \leq x \leq 0.82$, Bao et al.[2] discovered dynamic ferromagnetic spin correlations at high temperature and showed that the latter are replaced by antiferromagnetic spin fluctuations at low temperature. Long period structures associated with charge ordering were evidenced for $x \sim 0.80$ by Murakami et al.[3] whereas Chiba et al.[4] discovered ferromagnetism and especially large negative magnetoresistance for $x \geq 0.875$. Nevertheless the resistance ratio of these materials remains small compared to the hole-doped CMR manganites, i.e., typically, $R_0/R_{7T} \sim 3$ at 50 K. The recent study of the manganite $Ca_{1-x}Eu_xMnO_3$ for $x < 0.2$ showed also that the electron doping due to the substitution of the trivalent rare earth Eu(III) for calcium induces a magnetoresistance effect.[5] Here again the resistivity ratio remained small, i.e., $\rho_0/\rho_{12T} \sim 4$ at 30 K.

The recent systematic screening of the manganites $Ca_{1-x}Sm_xMnO_3$ for $0 \leq x \leq 0.2$ by Δx step of 0.01 has allowed colossal magnetoresistance properties to be evidenced for the first time,[6] as shown for $x = 0.15$, which exhibits resistance ratios ρ_0/ρ_{7T} of 10^2 and 10 at 50 and 100 K, respectively. These results are quite unexpected if one takes into account the average size of the interpolated cations $\langle r_A \rangle$, which is small compared to the one required for the appearance of the CMR effect in hole-doped manganites (see, for instance, refs 7−11). Thus, at this stage of the investigations, it is necessary to determine the chemical and crystallographic factors that govern the magnetotransport properties of the electron-doped materials. In the present work, we investigate systematically the magnetotransport properties of $CaMnO_3$ substituted with trivalent lanthanides (Ln = Pr, Nd, Eu, Gd, Ho) or with tetravalent elements (M = Ce, Th). From the comparison of the different properties resulting from these substitutions, including the results obtained for samarium,[6] we demonstrate that the electron concentration is a dominant factor, whereas size and mismatch effects influence the magnetotransport properties to a lesser degree.

Experimental Section

The $Ca_{1-x}Ln_xMnO_3$ oxides were prepared from mixtures of CaO, Ln_2O_3 or CeO_2 or $Th(CO_3)_2$, and MnO_2, prereacted in air at 1000 °C, pressed in bars form, heated at 1200 °C, and then sintered at 1500 °C for 12 h. Purity, homogeneity, and composition of the samples were checked by electronic diffraction (ED) and EDS analysis. The powder X-ray patterns were recorded by using a Philips diffractometer with Cu Kα radiation and scanning (0.02° step in 2θ) over the angular range $10° < 2\theta < 110°$ and were analyzed with the Fullprof program.[12] The "O_3" oxygen stoichiometry was determined by iodometric titration in the Sm series and by thermogravimetric analysis (at 800 °C under $Ar-H_2$ flow) for $x = 0$.

Resistivity measurements (four-probe method) were performed during cooling, the 7 T magnetic field being applied at 300 K. Magnetization curves were registered by means of a vibrating sample magnetometer. Samples were first zero-field cooled to 5 K, the temperature at which the magnetic field was applied, and data were registered during warming.

Results and Discussion

Structural Characterizations. All the samples are monophasic, as shown from the $Sm_{0.2}Ca_{0.8}MnO_3$ and $Th_{0.2}Ca_{0.8}MnO_3$ X-ray patterns (Figure 1). No impurities are detected by ED, and the EDS analysis confirms the nominal cationic compositions. The X-ray powder patterns of all these oxides can be indexed in the orthorhombic system space group *Pbnm* with $a \sim b \sim a_p\sqrt{2}$ and $c \sim 2a_p$. The evolution of the cell volume versus x (Figure 2) confirms that the doping elements have entered into the perovskite matrix and shows that regardless of whether Ln, Ce, or Th is used the volume increases with x. This effect is easily understood by the larger difference between Mn(III) and Mn(IV) (0.645 and 0.53 Å, respectively) than between Ca(II) and Ln(III) (1.18 and 1.132 Å, respectively, for Ca^{2+} and Sm^{3+} for instance). Moreover, at a constant x value, the cell

* To whom correspondence should be addressed. Electronic mail: maignan@crismat.ismra.fr.

(1) Bokov, V. A.; Grigoryan, N. A.; Bryzhina, M. F. *Phys. Stat. Sol.* **1967**, *20*, 745.
(2) Bao, W.; Axe, J. D.; Chen, C. H.; Cheong, S. W. *Phys. Rev. Lett.* **1997**, *78*, 543.
(3) Murakami, T.; Shindo, D.; Chiba, H.; Kikuchi, M.; Syono, Y. *Phys. Rev. B* **1997**, *55*, 1.
(4) Chiba, H.; Kikuchi, M.; Kusaba, K.; Muraoka, Y.; Syono, Y. *Solid State Commun.* **1996**, *99*, 499.
(5) Troyanchuk, I. O.; Samsonenko, N. V.; Szymczak, H.; Nabialek, A. *J. Solid State Chem.* **1997**, *131*, 144.
(6) Martin, C.; Maignan, A.; Damay, F.; Hervieu, M.; Raveau, B. *J. Solid State Chem.* **1997**, *134*, 198.
(7) Maignan, A.; Simon, Ch.; Caignaert, V.; Raveau, B. *Z. Phys. B* **1996**, *99*, 305.
(8) Millange, F.; Maignan, A.; Caignaert, V. Simon, Ch.; Raveau, B. *Z. Phys. B* **1996**, *101*, 169.
(9) Mahesh, R.; Mahendiran, R.; Raychaudhuri, A. K.; Rao, C. N. R. *J. Solid State Chem.* **1995**, *114*, 297; **1995**, *120*, 204.
(10) Hejtmanek, J.; Jirak, Z.; Sedmidubsky, D.; Maignan, A.; Simon, Ch.; Caignaert, V.; Martin, C.; Raveau, B. *Phys. Rev. B* **1996**, *54*, 11947.
(11) Fontcuberta, J.; Martinez, B.; Seffar, A.; Pinol, S.; Garcia-Munoz, J. L.; Obradors, X. *Phys. Rev. Lett.* **1996**, *76*, 1122.
(12) Rodriguez-Carvajal, J. In *Collected Abstracts of Powder Diffraction Metting*; Galy, J., Ed.; Toulouse, France, 1990; p 137.

S0897-4756(97)00781-3 CCC: $15.00
Published on Web 03/24/1998

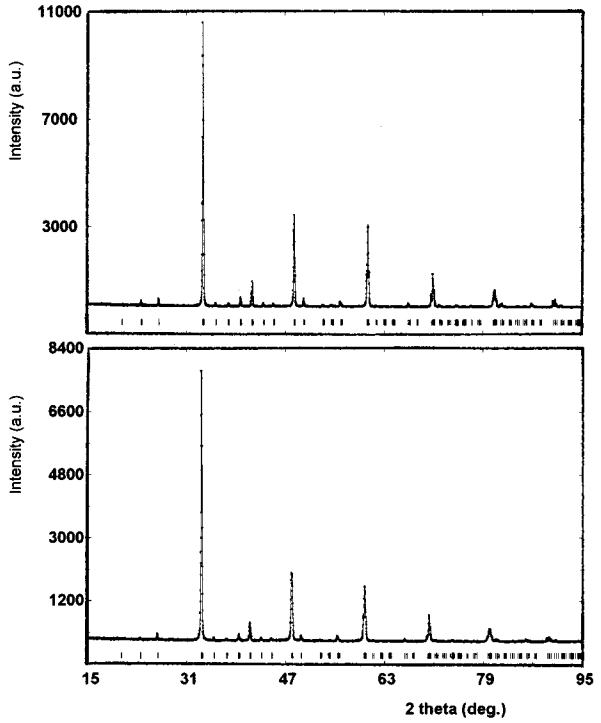

Figure 1. X-ray patterns for $Sm_{0.2}Ca_{0.8}MnO_3$ (top) and $Th_{0.2}Ca_{0.8}MnO_3$ (bottom).

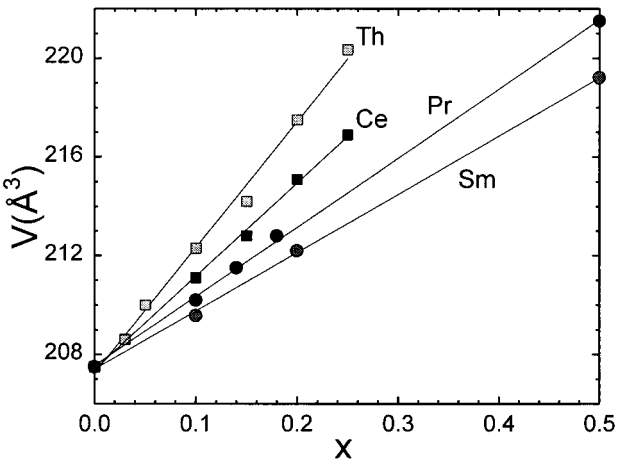

Figure 2. x dependence of the cell volume on $Ca_{1-x}Ln_xMnO_3$ (Ln = Th, Ce, Pr, and Sm).

volume decreases as the Ln^{3+} size decreases (from Pr to Ho), and the volume of the Th phase is definitely larger than that of the Ln manganites with Ln = Pr or Sm, despite the size of thorium, and significantly smaller than those of Pr(III) and Sm(III). Such a difference is explained by the Th valency: the introduction of one Th(IV) atom leads to the replacement of two Mn(IV) species by two Mn(III) species, whereas the introduction of one Ln(III) species corresponds to the replacement of one Mn(IV) by only one Mn(III) species. Thus the larger volume cell of the Th and Ce phases compared to the Pr phase is due to the increase of the Mn(III) content in the structure.

The Trivalent Lanthanide Series $Ca_{1-x}Ln_xMnO_3$. The systematic investigation of these compounds with Ln = Pr, Nd, Eu, Gd, and Ho for x values ranging from 0 to 0.2 by step of 0.01 shows that they all exhibit a behavior similar to that of the samarium phases $Ca_{1-x}Sm_xMnO_3$.[6]

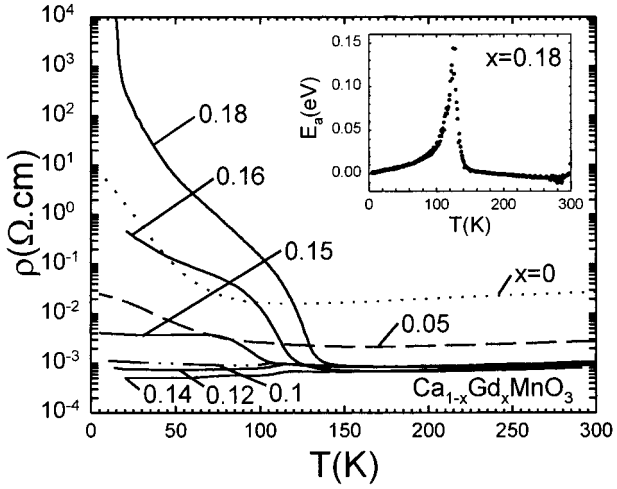

Figure 3. Temperature (T) dependence of the resistivity (ρ) for different compositions of $Ca_{1-x}Gd_xMnO_3$ samples (x values are labeled on the graph). Inset: activation energy versus T for $x = 0.18$.

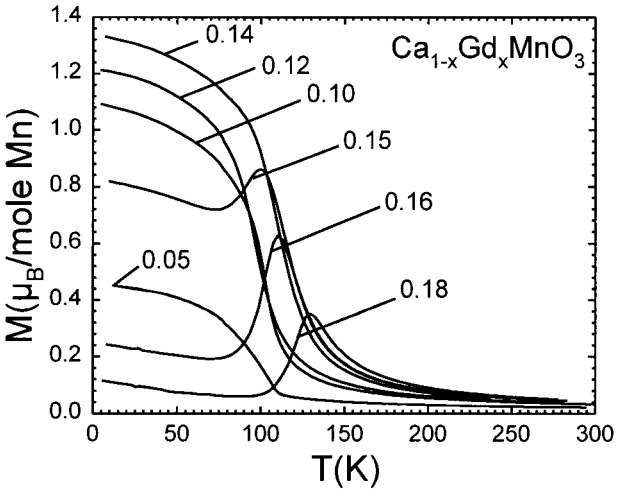

Figure 4. T dependence on the magnetization (M), registered under 1.45 T, for the same compounds.

(i) For low x values, $0 < x \leq 0.14$, a ferromagnetic state is induced at low temperature (Figure 4), i.e., for $T < 100$ K. Concomitantly, the resistance is lowered (Figure 3), tending to a semimetallic behavior (see, for instance, $x = 0.1-0.12$). Note, however, that the maximum value of the magnetic moment remains close to only 1.3 μ_B in a magnetic field of 1.45 T and that the maximum moment M_{5K} increases (Figure 5) as the size of the lanthanide decreases from 0.8 μ_B for Pr to 1.5 μ_B for Eu and seems to decrease again for Ho (1.2 μ_B).

(ii) For higher x values, $0.14 < x \leq 0.2$, the magnetic moment drops abruptly at low temperature (Figure 4, 5), leading to the antiferromagnetic state (Figure 4), whereas simultaneously the resistance is dramatically increased (Figure 3). In fact, in this range, the $\rho(T)$ curves (Figure 3) show a transition around 100−150 K from the semimetallic to the insulating state. The corresponding transition temperature T_R can be defined as the inflection point of the $\rho(T)$ curve (see example in inset of Figure 3). This transition coincides with the appearance of a rather sharp peak on the $M(T)$ curves (Figure 4), so that $T_{peak} \cong T_R$.

The $M(T)$ curves clearly show that there exists a competition between ferromagnetism and antiferromag-

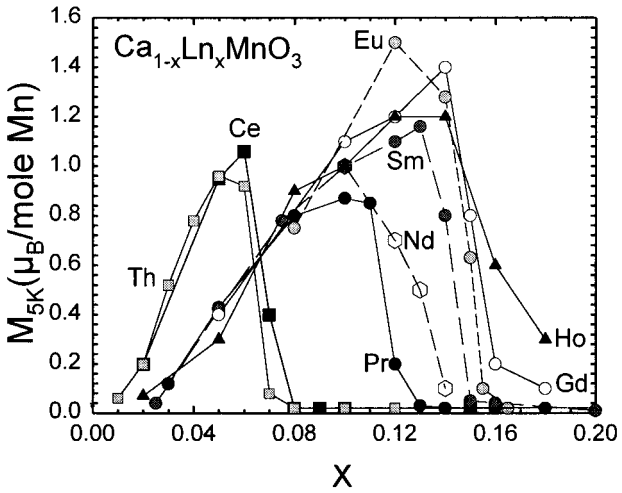

Figure 5. Magnetization, measured at 5 K (M_{5K}) versus x for the different series $Ca_{1-x}Ln_xMnO_3$ (Ln = Th, Ce, Pr, Nd, Sm, Eu, Gd, Ho).

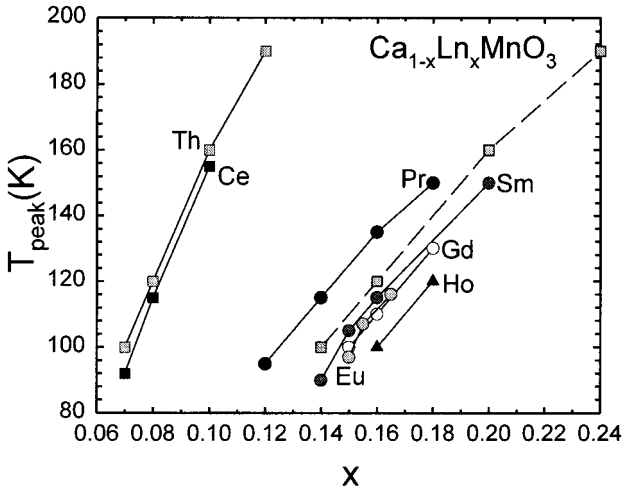

Figure 6. T_{peak}, obtained from the $M(T)$ curves, versus x.

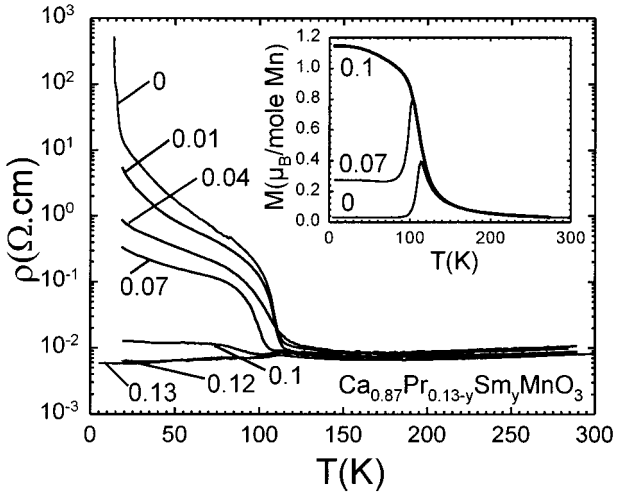

Figure 7. $\rho(T)$ curves for the $Ca_{0.87}Pr_{0.13-y}Sm_yMnO_3$ series (y values are labeled on the graph). Inset: corresponding $M(T)$ curves.

netism in these systems and that the ferromagnetic component goes through a maximum as x increases. Such a behavior can be interpreted on the basis of electronic delocalization and localization phenomena, in accordance with the $\rho(T)$ curves. For low x values, introduction of electrons on the e_g level of manganese leads to electronic delocalization and consequently favors the appearance of a ferromagnetic metallic (FMM) state at low temperature, so that the magnetic moment at 5 K increases in a first step with x. However, as x increases beyond a certain electron concentration (corresponding to $x \sim 0.12-0.14$), a localization of electrons appears (charge ordering or local charge ordering in the form of clusterization), so that antiferromagnetism is favored at the expense of ferromagnetism. Consequently, ferromagnetism cannot fully develop, and the saturation corresponding to a moment of 3.6 μ_B cannot be reached. Finally, the localization predominates for higher x values, and antiferromagnetism expands rapidly as x increases, so that the intensity of the peak of the $M(T)$ curves decreases abruptly (Figure 4). This interpretation agrees with the neutron diffraction study of $La_{1-x}Ca_xMnO_3$,[13] which shows charge-ordering phenomena for $x \cong 0.75$. Nevertheless, a complete structural study of all these oxides has to be performed in order to determine whether the charge-ordering phenomena that may appear are completely established or just involve local clusters.

It is now of interest to determine the factors which influence the transition temperature T_{peak} and the value of the magnetization. The $T_{peak}(x)$ curves (Figure 6) for the different Ln series show that for a given electron concentration T_{peak} is slightly affected by the size of the lanthanide. Indeed, one observes that for a fixed electron concentration x, the transition temperature T_{peak} decreases with the Ln size. In other words, as the mean ionic radius $\langle r_A \rangle$ of the interpolated cation increases, a higher electron concentration is necessary to replace the FMM state at the benefit of the antiferromagnetic insulating (AFMI) state. Thus, in contrast to the hole-doped manganites, the stability of the FMM state increases as the size of the interpolated cation decreases. This effect is illustrated by the magnetic and transport properties of the series $Ca_{0.87}Pr_{0.13-y}Sm_yMnO_3$ (Figure 7). The $M(T)$ curves (inset of Figure 7) show indeed that T_{peak} decreases as y increases so that the ferromagnetic state appears only for the smallest $\langle r_A \rangle$ values ($0.10 \le y \le 0.13$). Correlatively, the $\rho(T)$ curves (Figure 7) show that T_R decreases as y increases and especially that the resistivity at low temperature, below T_R, decreases as $\langle r_A \rangle$ decreases, the semimetallic state being reached for the lowest $\langle r_A \rangle$ values corresponding to $0.10 \le y \le 0.13$. Note, however, that the size effect alone cannot explain the changes of properties that are observed since the series $Ca_{1-x}Pr_xMnO_3$—for which $\langle r_A \rangle$ is kept constant—exhibit also the transition from a FMM to an AFMI state as x increases. It must also be emphasized that the mismatch due to the size difference between the A site cations may also influence these properties. The latter, characterized by the variance σ^2 defined as $\sigma^2 = \sum y_i r_i^2 - \langle r_A \rangle^2$ according to Attfield et al.,[14] although it increases from Pr to Ho, remains rather small for $x < 0.20$, so that its influence cannot be evaluated easily (Table 1).

(13) Wollan, E. O.; Koehler, W. C. *Phys. Rev.* **1955**, *100*, 543.
(14) Rodriguez-Martinez, L. M.; Attfield, J. P. *Phys. Rev. B* **1996**, *54*, 15622.
(15) Shannon, R. D. *Acta Crystallogr.* **1976**, *A32*, 751.

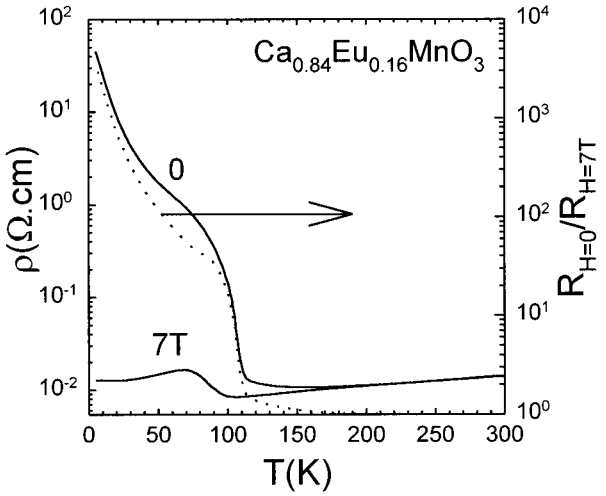

Figure 8. Temperature dependence on ρ in 0 and 7 T (left axis) and magnetoresistance ratio ρ_0/ρ_{7T} (right axis) for $Ca_{0.84}Eu_{0.16}MnO_3$.

Table 1. $\langle r_A \rangle$ (According to Shannon[15]), σ^2, and Resistance Ratio ρ_0/ρ_{7T} for x_{opt} in Each Series $Ca_{1-x}Ln_xMnO_3$

				ρ_0/ρ_{7T}		
Ln	x_{opt}	$\langle r_A \rangle$ (Å)	σ^2 (Å^2)	5 K	50 K	100 K
Th	0.08	1.173	5.96×10^{-4}	50	4	3
Ce	0.08	1.167	1.88×10^{-3}	6000	5	4
Pr	0.135	1.18	1.168×10^{-7}	400	8	4.5
Nd	0.135	1.178	3.37×10^{-5}	1200	20	5
Sm	0.15	1.173	6.7×10^{-3}	1000	100	10
Eu	0.16	1.170	4.84×10^{-4}	3500	110	15
Gd	0.16	1.168	7.16×10^{-4}	500	40	10
Ho	0.16	1.163	1.57×10^{-3}	14	12	5

The $\rho(T)$ curves registered in a magnetic field of 7 T show that for each lanthanide there exists an optimal x value for which the CMR effect is maximum. Just below x_{opt} the material is ferromagnetic, its magnetic moment being close to 1 μ_B, and it exhibits a semimetallic behavior so that its negative magnetoresistance is low. In contrast, at x_{opt} the competition between ferromagnetism and antiferromagnetism reaches its maximum and, as a result, the resistance ratio (RR) is high. Above x_{opt}, the increase of antiferromagnetism tends to suppress the magnetoresistance effect, and consequently RR decreases rapidly. Thus, the x range where the material exhibits CMR effects is rather narrow. This explains why, for the series $Ca_{1-x}Eu_xMnO_3$, resistance ratios of only 4 at 30 K under 12 T were detected.[5] In fact, for the latter series, resistance ratios of 110 at 50 K and of 15 at 100 K are observed in a magnetic field of 7 T (Figure 8) for the value $x_{opt} = 0.16$. For each series, the x_{opt} values and the corresponding RR at three temperatures (T = 5, 50, and 100 K) are listed in Table 1. One observes that x_{opt} increases slightly from 0.135 for Pr to 0.16 for Eu as the size of the lanthanide decreases and then remains constant down to Ho. Correlatively, as the size of the interpolated cation decreases, the RR increases from 8 at 50 K for Pr to 110 for Eu and then decreases down to 40 and 12 for Gd and Ho, respectively.

The Tetravalent-Element-Doped Manganites $Ca_{1-x}Ce_xMnO_3$ and $Ca_{1-x}Th_xMnO_3$. Tetravalent thorium, owing to its size close to that of the praseodymium, is a potential substituting element for manganites. Moreover, thanks to its tetravalent character, it is susceptible to introduce twice more electrons per substituting atom than lanthanides. For this reason, we have explored the manganites $Ca_{1-x}Th_xMnO_3$ on the Mn(IV)-rich side, i.e., for $x \leq 0.20$. The $M(T)$ curves registered under 1.45 T (Figure 9) and the $\rho(T)$ curves (inset of Figure 9) show for the first time that the substitution of $CaMnO_3$ with thorium leads to the same effect as that obtained with trivalent lanthanides. For low x values ($x \leq 0.05$), ferromagnetism increases slowly with x at low temperature ($T < 100$ K) and reaches a magnetic moment of 1 μ_B at $x \cong 0.05$ (Figure 9), whereas for these compositions and temperature ranges the resistivity decreases slowly as x increases up to $x = 0.04$ and then increases slightly. For $x \leq 0.07$, a peak appears on the $M(T)$ curves whose intensity decreases as x increases. This peak broadening occurs for the larger x values ($x \sim 0.10-0.12$). As for the trivalent lanthanides, T_{peak} increases with x (Figure 9) and coincides with the transition temperature T_R deduced from the $\rho(T)$ curves which evidence also a transition from the semimetallic to semiconducting state as T decreases (inset of Figure 9). Thus, the $Ca_{1-x}Th_xMnO_3$ samples exhibit, like the $Ca_{1-x}Ln_xMnO_3$ samples, a competition between ferromagnetism and antiferromagnetism at low temperature. But the most important feature concerns the evolution of T_{peak} vs x (Figure 6). One indeed observes that the transition corresponding to T_{peak} (T_R) appears for much lower thorium contents ($x \sim 0.07-0.12$) compared to trivalent lanthanides ($x \sim 0.135-0.20$). Such a behavior is easily explained by the tetravalent character of thorium which introduces an electron concentration twice higher than that introduced per atom by trivalent lanthanides. Then, the behavior of Th(IV) can be better compared to that of trivalent lanthanides by plotting T_{peak} vs $2x$, leading to the dashed line on Figure 6. From this comparison, it can be seen that, considering the electron concentration (i.e., Mn(III) concentration), the thorium-substituted phases exhibit a behavior similar to that of the trivalent lanthanides. These results demonstrate that the electron concentration is a predominant factor for the magnetic and transport properties of the electron-doped manganites. This behavior is also confirmed from the graph of the magnetization at 5 K versus x (Figure 5)

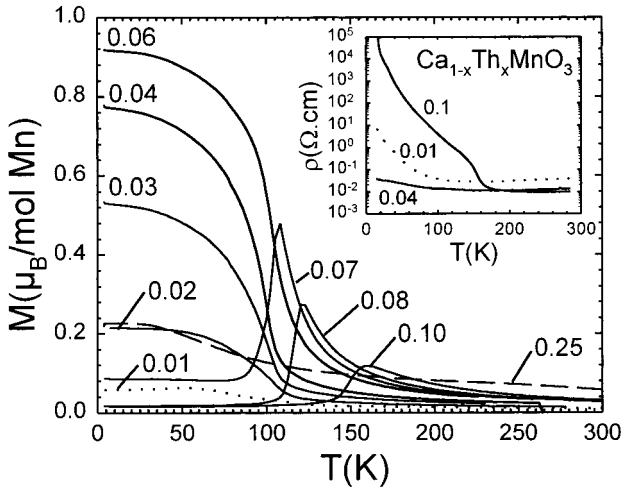

Figure 9. $M(T)$ curves for $Ca_{1-x}Th_xMnO_3$. Inset: corresponding $\rho(T)$ curves.

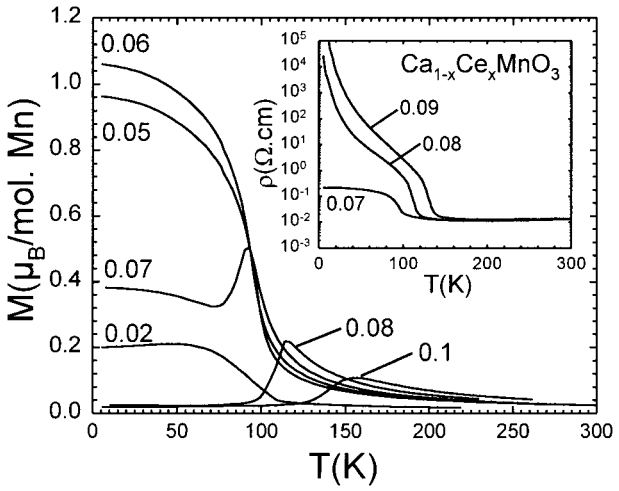

Figure 10. $M(T)$ curves for $Ca_{1-x}Ce_xMnO_3$. Inset: corresponding $\rho(T)$ curves.

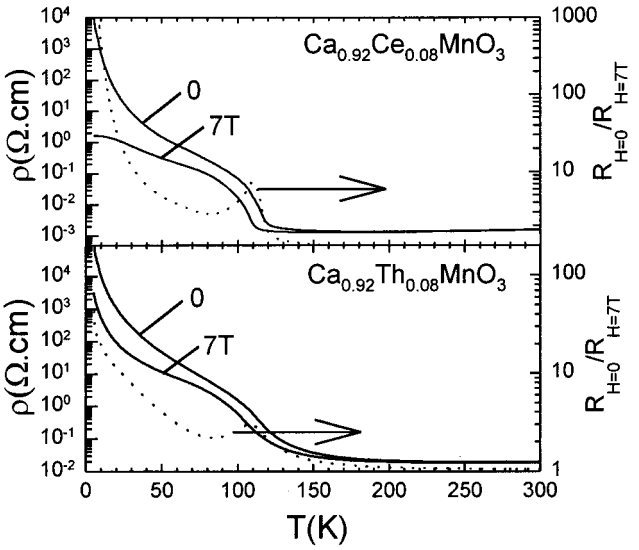

Figure 11. $\rho(T)$ curves under 0 and 7 T (left axis) and ρ_0/ρ_{7T} (T) curves (right axis) for $Ca_{0.92}Ce_{0.08}MnO_3$ (upper part) and $Ca_{0.92}Th_{0.08}MnO_3$ (lower part).

which shows that the $M_{5K}(x)$ curves for Ln(III)-doped phases are shifted by a factor of 2 along x with respect to the Th-substituted phase.

From this comparison between Th(IV) and Ln(III) dopants, it is possible to know whether cerium can be introduced in the perovskite matrix in the form of Ce(III) or Ce(IV). The study of the cerium-substituted samples $Ca_{1-x}Ce_xMnO_3$ shows that their crystallographic cell is similar to those of thorium- and Ln(III)-doped calcium manganites. The volume cell increases with x as for thorium, but remains significantly smaller than that of the thorium phases and larger than that of the Ln(III) phases (Figure 2). Therefore, the structural evolution does not allow the oxidation state of cerium—Ce(III) or Ce(IV)—to be determined. Nevertheless, the $M(T)$ curves (Figure 10) and the $\rho(T)$ curves (inset of Figure 10) clearly show that the Ce-substituted phases exhibit magnetic and transport properties close to those of the Th manganites. At low temperature (T < 100 K), ferromagnetism indeed increases as x increases up to $x = 0.06$, and the peak characteristic of the competition between ferromagnetism and antiferromagnetism appears exactly at the $x = 0.07$ value, as in case of the Th-substituted phases. Correlatively the $\rho(T)$ curves (inset of Figure 10) show a transition from the semimetallic to the insulating state for the same x values. Thus, the $T_{peak}(x)$ curves (Figure 6), as well as the $M_{5K}(x)$ curves (Figure 5), are very close to those of the Th samples, i.e., they are shifted by a factor $^1/_2$ along x with respect to the Ln(III) samples. These results demonstrate that cerium is tetravalent in these perovskites.

From this investigation, it is then possible to foresee that the phases $Ca_{1-x}Th_xMnO_3$ and $Ca_{1-x}Ce_xMnO_3$ will exhibit CMR properties and that the optimal x value will be close to $x_{opt} \cong 0.08$ for both series. A systematic scanning of the magnetoresistance properties versus x by step of 0.01 confirms this forecast. The $\rho(T)$ curves registered under 7 T for both oxides, with $x_{opt} = 0.08$ (Figure 11), show similar RR.

Conclusion

Among the three important factors governing the CMR properties of Mn(III)-rich compounds—hole carrier density, average size of the interpolated cation $\langle r_A \rangle$, and A-site cationic size mismatch—the electron carrier density is found to be the predominant one for the Mn(IV)-rich compositions $Ca_{1-x}Ln_xMnO_3$ and $Ca_{1-x}Th_xMnO_3$ ($0 \le x \le 0.2$). As x increases from $x = 0$, a ferromagnetic metallic (FMM) state below $T_C \sim 130$ K is first induced regardless of the substituting element (lanthanide or thorium). Nevertheless, this effect goes faster for Th and Ce in agreement with their IV formal oxidation states. Beyond a critical x_{opt} value, an AFMI state competes with the FMM one so that the magnetization curves exhibit a peak, while the magnetoresistance reaches its maximum amplitude for x_{opt}. The electron concentration range around x_{opt}, within which CMR properties are exhibited, is very narrow, since as soon as $x > x_{opt}$, the AFMI state is strong enough to resist to the magnetic field application (up to 7 T). Finally, the most important result of the study is that the same trend with the electron concentration is observed whatever the substituting element (lanthanide or thorium). This is illustrated by the room-temperature values that are all around $\rho_{300K} = 10^{-3}$ Ω cm for the optimum concentration in each series and by the resistivity ratios (ρ_0/ρ_{7T}) that can reach several thousands at 5 K for Sm(III), Eu(III), and Ce(IV).

CM970781B